Molecular Dynamics Study of Structure and Transport of Water and Hydronium Ions at the Membrane/Vapor Interface of Nafion

Myvizhi Esai Selvan,[†] Junwu Liu,[†] David J. Keffer,*[,†] Shengting Cui,[†] Brian J. Edwards,[†] and William V. Steele[†,‡]

Chemical and Biomolecular Engineering Department, 327 Dougherty Engineering Building, 1512 Middle Drive, University of Tennessee, Knoxville, Tennessee 37996-2200, and Nuclear Science and Technology Division, Oak Ridge National Laboratory (ORNL), Oak Ridge, Tennessee 37831-6273

Received: July 17, 2007; In Final Form: October 19, 2007

Through the use of molecular dynamics simulation, we examine the structural and transport properties of water and hydronium ions at the interface of a Nafion polymer electrolyte membrane and a vapor phase. The effect of humidity was studied by examining water contents of 5%, 10%, 15%, and 20% by weight. We observe a region of water depletion in the membrane near the vapor interface. We report the vehicular diffusion of hydronium ions and water as components parallel and perpendicular to the interface. In the interfacial region, for hydronium ions, we find that the component of the vehicular diffusivity parallel to the interface is largely unchanged from that in the bulk hydrated membrane, but the component perpendicular to the interface has increased, due to local decrease in density. We find similar behavior with water in the interfacial region. On the basis of these diffusivities, we conclude that there is no observable additional resistance to mass transport of the vehicular component of water and hydronium ions due to the interface. In terms of structure at the interface, we find that there is a decrease in the fraction of fully hydrated hydronium ions. This translates into a lower probability of forming Eigen ions, which are necessary for structural diffusion. Finally, we observe that the hydronium ions display a preferential orientation at the interface with their oxygen atoms exposed to the vapor phase.

I. Introduction

In order to have a well-founded scientific basis for fuel cell design, one would benefit from a molecular-level understanding of the transport processes governing the movement of hydrogen, oxygen, water, and protons in the fuel cell.[1] Perhaps one of the least-understood molecular-level process in the fuel cell involves the catalyst particle.[2,3] On the anode, the particle must participate in three transport functions: (1) adsorbing molecular hydrogen, (2) conducting electrons to the electrode via the catalyst support, and (3) transport of protons into the hydrated polymer electrolyte membrane (PEM). If the molecular hydrogen arrives in the vapor phase within a pore of the electrode, then the catalyst particle must have interfaces with three phases: the vapor phase, the solid phase of the support, and the hydrated membrane phase.

The nanoscale structure of the electrode/electrolyte interface is a function of the manufacturing process, including the amount of recast Nafion used in the electrode and the manner in which the catalyst particles are deposited. In Figure 1, we present an idealized graphic representing a small portion of the membrane electrode assembly (MEA) at the interface of the electrode and the PEM. In this graphic, molecular hydrogen diffuses in the vapor phase through a pore in the midst of the carbon support. We can identify four subsystems of interest in terms of proton transport: (1) the "bulk" hydrated PEM, (2) the membrane/vapor interface, (3) the membrane/vapor/support interface, and (4) the membrane/vapor/catalyst interface. The geometry of the schematic in Figure 1 is certainly idealized, but the presence of the four systems containing the PEM is relevant, regardless of the larger scale geometry.

There has been significant progress toward understanding the proton transport mechanism within the bulk hydrated membrane (region 1 in Figure 1) from experiment,[4−6] molecular-level simulation,[1,7−28] and macroscopic models.[29−31] What has emerged from this body of work is a partial understanding that the Grotthuss mechanism responsible for structural diffusion of protons is perturbed within the confined and highly acidic environment of a proton exchange membrane. This understanding is not as yet developed sufficiently to allow for the theoretical prediction of the relationship between proton conductivity and polymer electrolyte architecture.

The other three regions in Figure 1 have received substantially less attention.[32] Although there are modeling studies describing the water transport phenomena in the gas diffusion layer (GDL), catalyst layer (CL), and PEM,[33,34] they do not provide a molecular-level mechanism for proton transport. In this work, we focus on a description of the membrane/vapor interface, examining structural and transport properties. We model Nafion because it is the prototypical PEM used in fuel cells. Our objective is to determine if there is intrinsic resistance to the mass transport of water and hydronium ions across the membrane/vapor interface. A complementary molecular dynamics study of regions 3 and 4 in Figure 1 is currently under review.[35]

The remainder of the paper is organized as follows. In Section II, we review the theory we employ to determine the perpendicular and parallel components of the vehicular diffusivity of water and hydronium in the interfacial region. Section III

* Author to whom correspondence should be addressed. E-mail: dkeffer@utk.edu. Tel: (865)-974-5322.
† University of Tennessee.
‡ ORNL.

10.1021/jp075611t CCC: $40.75
Published on Web 01/24/2008

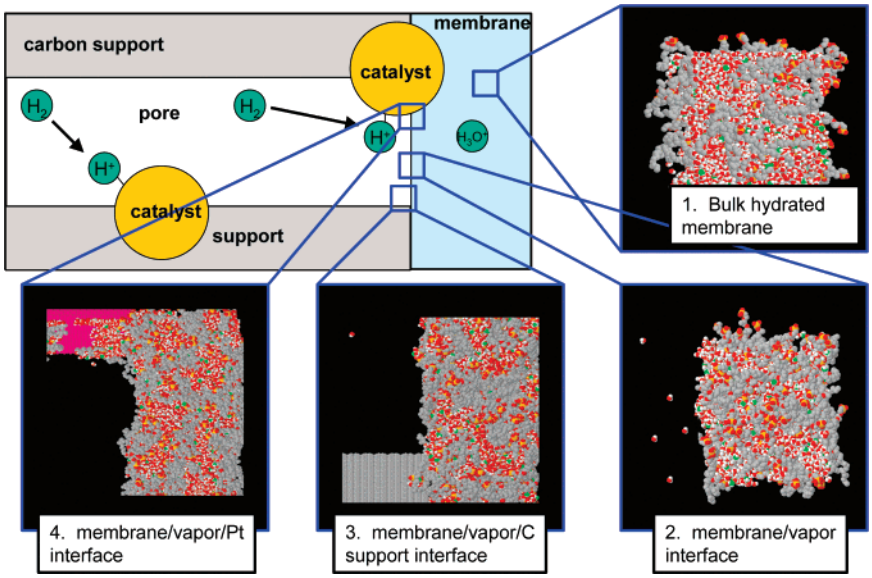

Figure 1. Idealized schematic illustrating the molecular-level interfaces present at the electrode/electrolyte interface of the membrane electrode assembly.

describes our model parameters and simulation technique. In Section IV, we present our results and discussion of the structural and transport properties of water and protons at the membrane/vapor interface. Finally, we summarize our conclusions in Section V.

II. Interfacial Diffusivities

The measurement of the self-diffusivities of components in mixtures via equilibrium molecular dynamics (MD) simulation is a standard procedure when the mixture is homogeneous.[36,37] On the basis of the theory of time correlation functions,[38,39] one can write expressions for the self-diffusivity in terms of a Green−Kubo velocity autocorrelation function (VACF) or equivalently using the Einstein relation in terms of the mean square displacement (MSD). In a mixture, we understand that the self-diffusivity corresponds not to a pure component property but rather to a gradient-free asymptote; that is, where each component has a distinct self-diffusivity that is a function of the thermodynamic state, including composition.[40] Through the Darken equation,[41] one can relate self-diffusivities to Fickian diffusivities, which can be used in macroscopic transport equations that describe mass transfer. There are advantages to obtaining the self-diffusivity in MD, primarily due to the fact that it is a single-particle correlation function (as opposed to the Fickian diffusivity, which is an all-particle correlation function). Consequently, these can be obtained with far greater statistical reliability.[42] If proper care is taken to ensure that the same reference frame is applied to diffusion in the molecular simulation and the macroscopic model, then the diffusivities obtained from MD are immediately applicable at the coarser scale.[43]

The measurement of self-diffusivities in a heterogeneous system deserves separate treatment. Before we begin, we should clearly define when we shall consider a system homogeneous or heterogeneous. There are two distinct phases in hydrated Nafion: a hydrophobic phase composed of the polymer backbones; and a hydrophilic phase consisting of hydrated sulfonic acid groups bound to the end of the polymer side chains, hydrated protons and water. Our previous simulation of bulk hydrated Nafion[14] shows the morphology of a tortuous aqueous nanonetwork distributed within the polymer. This system is heterogeneous at the nanoscale. However, the water molecules are considered to be located exclusively in the hydrophilic phase. Therefore, from the point of view of a water molecule, there is only one phase, deformed into a dynamic morphology by a region of inaccessible volume. As a result, in this work we can treat the bulk hydrated membrane as a homogeneous system with respect to the transport properties of the water molecules and hydronium ions.

We should note that the specific morphology of the aqueous nanophase is generally considered to be dynamic in time. The fluctuations in the connectivity of various aqueous clusters can certainly influence the overall diffusivity of water and hydronium ions and consequently the conductivity of the membrane. Although the lifetime of these aqueous clusters is not known, we will see from the variation in the density profiles below that it is larger than the time scale of our simulations (4 ns). Therefore, in obtaining even the self-diffusivities in the bulk hydrated membrane, we assume that the system is large enough to sample water and hydronium molecules in various environments (at the center and at the edges of aqueous clusters) to provide a meaningful average diffusivity.

When we introduce a microscopic interface between the PEM and a vapor phase, a water molecule can reside in a variety of environments ranging from the aqueous component of the bulk membrane, through the interface, and into the bulk vapor. This environment changes sharply but continuously. For simplification of description, we shall consider this system to be composed of three regions: (1) bulk membrane, (2) interface, and (3) bulk vapor.

An instantaneous property like the density distribution can be determined straightforwardly from an MD simulation by knowledge of the instantaneous position of each particle. Therefore, with relative ease one can generate densities of water in each of the phases, bulk membrane, interface, and bulk vapor. However, a time correlation function, which relies on trajectories evolving over time, cannot be assigned unambiguously to a particular region of the system. The trajectory of a single particle can move through various regions. If one uses either the VACF or MSD to compute the self-diffusivity, then one is required to examine the behavior in the infinite time limit. Because particles can move between phases before this limit is reached, one cannot obtain region-specific self-diffusivities, unless one limits the analysis to molecules that spend the entire duration of the

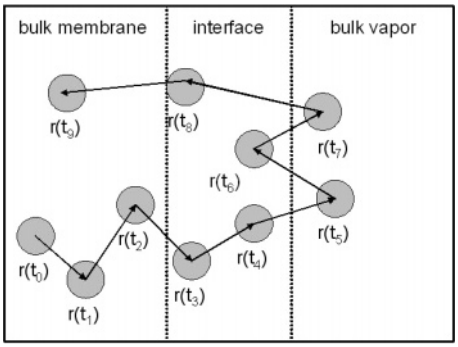

Figure 2. Schematic illustrating the difficulty of directly calculating an interfacial self-diffusivity from a multiphase simulation using either the VACF or MSD.

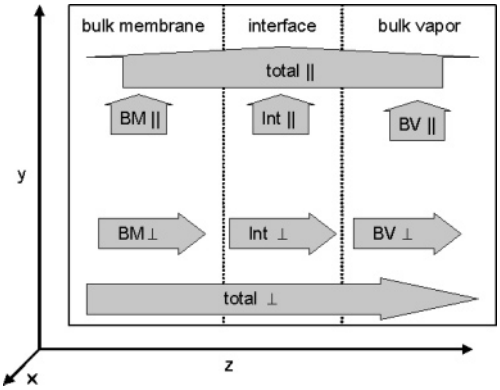

Figure 3. Schematic illustrating the modes of transport in the three-phase system.

simulation in a single phase; however, this amounts to throwing away the information from many of the particles in the simulation. In Figure 2, we provide a conceptual example of a trajectory that moves through many phases without reaching the infinite-time limit in any one individually. Certainly, one can use the conventional VACF or MSD to obtain the self-diffusivity of the total system, averaged over all regions.

In this work, we rely on the knowledge of the behavior of transport properties in series and in parallel. In Figure 3, we show a schematic of a system with a planar interface. The three phases, bulk membrane (BM), interface (I), and bulk vapor (BV), present three resistances to mass transport, which are in series in the z dimension and in parallel in the x and y dimensions. In the analysis that follows, we assume that the morphology of the aqueous nanophase is static. This is reasonable if we again assume that our simulation volume is sufficiently large to capture the average environment of the water and hydronium ions present.

We begin the analysis with Fick's law for a binary, isothermal system with variation in one-dimension

$$j_A = -\rho D \frac{dw_A}{dz} \tag{1}$$

where j_A is the diffusive mass flux of component A relative to the center-of-mass motion of the system, ρ is the mass density, w_A is the mass fraction of component A, z is the spatial coordinate, and D is the diffusivity. For the binary case, under the assumptions listed above, there is only one diffusivity, $D = D_A = D_B$.

In the case of mass transfer in parallel, dw_A/dz the driving force is the same in each region because there can be no mass accumulation in any region at steady state and also each region shares a common boundary with the other (i.e., the final boundary of the bulk membrane is the initial boundary of the interface). If we write eq 1 for each of the three phases, as well as for the total system (T), and equate the gradients, then we have

$$\left.\frac{dw_A}{dz}\right|^{T} = \left.\frac{dw_A}{dz}\right|^{BM} = \left.\frac{dw_A}{dz}\right|^{I} = \left.\frac{dw_A}{dz}\right|^{BV} \tag{2}$$

The total rate of transport is the sum of the rate of transport in each of the three regions

$$A_z^T j_A^T = A_z^{BM} j_A^{BM} + A_z^I j_A^I + A_z^{BV} j_A^{BV} \tag{3}$$

where A_z^J is the cross-sectional area of region J. Combining eqs 1−3 leads to an expression for the total diffusivity parallel to the interface

$$D_{||}^T = \frac{A_z^{BM}\rho^{BM}D_{||}^{BM} + A_z^I\rho^I D_{||}^I + A_z^{BV}\rho^{BV}D_{||}^{BV}}{A_z^T\rho^T} \tag{4}$$

For the case of mass transport in series (perpendicular to the interface), at steady state, the flux in eq 1 is the same for each region and for the system total. Also, the cross-sectional area of each region is a constant. Therefore, we have

$$j_A^T = j_A^{BM} = j_A^I = j_A^{BV} \tag{5}$$

Furthermore, the total driving force is the sum of the driving forces across each region

$$\left.\frac{dw_A}{dz}\right|^{T} = \left.\frac{dw_A}{dz}\right|^{BM} + \left.\frac{dw_A}{dz}\right|^{I} + \left.\frac{dw_A}{dz}\right|^{BV} \tag{6}$$

Combining eqs 1, 5, and 6 leads to an expression for the total diffusivity perpendicular to the interface

$$\frac{1}{\rho^T D_\perp^T} = \frac{1}{\rho^{BM} D_\perp^{BM}} + \frac{1}{\rho^I D_\perp^I} + \frac{1}{\rho^{BV} D_\perp^{BV}} \tag{7}$$

The goal of this work is to determine the components of the interfacial diffusivity, $D_{||}^I$ and $D_\perp^I$. To do this, we must know all four of the densities, the four cross-sectional areas, and the other six diffusivities that appear in eqs 4 and 7. Because the BM and BV phases are isotropic, we know that $D^{BM} = D_\perp^{BM} = D_{||}^{BM}$ and $D^{BV} = D_\perp^{BV} = D_{||}^{BV}$. This leaves four densities, four areas, and four diffusivities to be determined for each state point.

We determine these properties in the following manner. In our earlier MD simulations of the BM phase, we have reported the ρ^{BM} and D^{BM} of water at four degrees of hydration corresponding to nominal water weight percents of 5%, 10%, 15%, and 20%.[14] In this work, we performed extensive MD simulations of the BM/I/BV system, from which we collected ρ^T, ρ^I, ρ^{BV}, $D_\perp^T$, and $D_{||}^T$.

There remains some ambiguity in the determination of the density of a region and the appropriate cross-sectional area. First we consider strictly a BM simulation, as reported previously.[14] In this case, there is an aqueous nanonetwork through which diffusion of water occurs. There is no water transport in the hydrophobic region. The question becomes whether one should report the bulk density, that is, the mass of water per simulation volume, $N_{H_2O}m_{H_2O}/V_{sim}$, or the density of water in the nanochannels, $N_{H_2O}m_{H_2O}/V_{chan}$, because they exclusively transport the water. Likewise, what is the appropriate area to use, $A_{sim} = V_{sim}/L$ or $A_{chan} = V_{chan}/L$, where L is the length of the simulation

box in the direction of transport? All other things being equal, one would much rather use the simulation volume and area because they can be determined unambiguously. Also, one should acknowledge that the estimation of the volume of the aqueous nanonetwork is not trivial.

To resolve this issue, we can consider the BM region itself to be an isotropic phase composed of two subregions, one composed of polymer (P) with water density, $\rho_P^{BM} = 0$, volume, V_P, and water diffusivity, $D_P^{BM} = 0$. The second subregion is the network of aqueous channels (chan) with $\rho_{chan}^{BM} = N_{H_2O} m_{H_2O}/V_{chan}$; volume, V_{chan}, and water diffusivity, D_{chan}^{BM}. Because the two subregions are parallel (as opposed to being in series), we use the same logic employed previously to arrive at eq 4 for the total diffusivity in the BM region

$$D^{BM} = \frac{A_{z,P}^{BM}\,\rho_P^{BM}\,D_P^{BM} + A_{z,chan}^{BM}\,\rho_{chan}^{BM}\,D_{chan}^{BM}}{A_{z,T}^{BM}\,\rho_T^{BM}} = \frac{A_{z,chan}^{BM}\,\rho_{chan}^{BM}\,D_{chan}^{BM}}{A_{z,T}^{BM}\,\rho_T^{BM}} = D_{chan}^{BM} \quad (8)$$

Therefore, we see that the total diffusivity of the BM region is exactly the diffusivity of the aqueous subregion. There is no need to be concerned with defining channel volumes because those factors cancel each other.

For the multiphase system with the BM, I, and BV regions, the solution is not so simple because the density is not zero in each of the phases. Our simulation box is a right parallelepiped with geometry defined by side magnitudes L_x, L_y, and L_z and angles $\theta_{xy} = \theta_{xz} = \theta_{yz} = 90°$. The interface lies in the *xy* plane. Along the *z* axis, we define distances corresponding to each region, such that the sum of these regions is L_z, $L_z = L_z^{BM} + L_z^{I} + L_z^{BV}$. Therefore, the volume of region *J* is $V^J = L_z^J L_x L_y$. The density of region *J* is then determined knowing the number of water molecules in region *J*, $N_{H_2O}^J$, and the region volume. If we insert these definitions into eq 4 for diffusion parallel to the interface, then we obtain

$$D_{||}^{T} = \frac{N_{H_2O}^{BM}\,D_{||}^{BM} + N_{H_2O}^{I}\,D_{||}^{I} + N_{H_2O}^{BV}\,D_{||}^{BV}}{N_{H_2O}^{T}} = \chi_{H_2O}^{BM}\,D_{||}^{BM} + \chi_{H_2O}^{I}\,D_{||}^{I} + \chi_{H_2O}^{BV}\,D_{||}^{BV} \quad (9)$$

where $\chi_{H_2O}^J \equiv N_{H_2O}^J/N_{H_2O}^T$ is the fraction of water molecules residing in region *J*. Again, we see that there is no need to know the volume of the individual regions, only the distribution of water among them. The distribution of the water among the regions is an unambiguous output from the MD multiphase simulation.

Similarly, if we put these definitions into eq 7 for diffusion perpendicular to the interface, then we have

$$\frac{1}{D_\perp^T} = \frac{1}{\frac{\chi_{H_2O}^{BM}}{\psi_z^{BM}} D_\perp^{BM}} + \frac{1}{\frac{\chi_{H_2O}^{I}}{\psi_z^{I}} D_\perp^{I}} + \frac{1}{\frac{\chi_{H_2O}^{BV}}{\psi_z^{BV}} D_\perp^{BV}} \quad (10)$$

where $\psi_z^J \equiv L_z^J/L_z$ is the distribution of volume between the three phases. The specification of L_z^J is arbitrary but must be chosen consistently in the definitions of $\chi_{H_2O}^J$ and ψ_z^J.

In the case of hydronium, following the same procedure and arguments, eqs 9 and 10 can be rewritten as

$$D_{||}^{T} = \chi_{H_3O}^{BM}\,D_{||}^{BM} + \chi_{H_3O}^{I}\,D_{||}^{I} \quad (11)$$

$$\frac{1}{D_\perp^T} = \frac{1}{\frac{\chi_{H_3O}^{BM}}{\psi_z^{BM}} D_\perp^{BM}} + \frac{1}{\frac{\chi_{H_3O}^{I}}{\psi_z^{I}} D_\perp^{I}} \quad (12)$$

because there are no hydronium ions in the vapor phase; that is, $N_{H_3O}^{BV} = \chi_{H_3O}^{BV} = 0$. Using eqs 11 and 12, we calculated the parallel and the perpendicular components of the self-diffusivity of hydronium in the interfacial region.

Equations 9−12 are macroscopic equations derived from continuum theory and require Fickian diffusivities for binary systems. Our MD simulations are molecular-level descriptions that deliver self-diffusivities for a ternary (Nafion, hydronium ions, and water) system. At this time, we accept these limitations.

III. Simulation Methods

In the simulations, we have used the same interaction potentials for the polymer electrolyte, water, and hydronium molecules as used earlier in the simulations of the bulk hydrated membrane.[14] In summary, each polymer unit consists of three monomers. Each ionomer has three side chains, 46 CF_2 groups along the backbone, and CF_3 group at each end. The justification of this model and the successful comparison with similar simulations performed with longer chains has been discussed previously.[14] The water is modeled using the TIP3P model with a flexible OH bond, while the model for hydronium ions is similar to that used by Urata et al.[27]

As was the case in the bulk hydrated membrane simulations, we have examined the properties of the system for water contents of 5%, 10%, 15%, and 20% by weight of the hydrated Nafion polymer electrolyte. These correspond to the λ ratio (defined as the number of water molecules to the number of SO_3^- groups) of 3.44, 5.42, 8.63, and 11.83, respectively.

The equilibrated configurations from the previous simulations[14] were used as a portion of the initial configuration in the present simulation. Specifically, we chose to increase the simulation volume by a factor of 2 in all directions. Therefore, we quadrupled the number of Nafion, water, and hydronium ions in these interfacial simulations, which leads to doubling in system size in the *x* and *y* dimensions. In the *z* dimension, we initially left the extra volume empty and allowed it to be filled with vaporized water molecules through equilibration during the simulation. This results in a simulation with 256 Nafion ionomers containing 768 SO_3^- groups as well as 768 H_3O^+ ions and 2640 to 9088 water molecules, depending upon the humidity level. Each configuration was equilibrated for 2 ns, and the data production runs were carried on for an additional 2 ns. The total system densities (including vapor volume), simulation length of the box, and the number of molecules of each type used are listed in the Table 1.

TABLE 1: Simulation Details for the Different Water Contents

water content (wt %)	number of nafion molecules	number of water molecules	number of hydronium ions	length of the simulation box (Å)	density (g/cm^3)
5	256	2640	768	117.29356	0.975
10	256	4160	768	120.13265	0.935
15	256	6624	768	123.48771	0.9
20	256	9088	768	126.67535	0.87

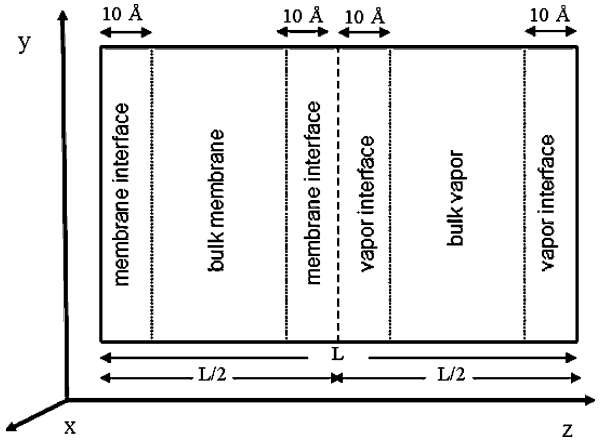

Figure 4. Schematic illustrating the division of the simulation box into four regions.

Simulations were carried out at constant NVT for the system. The 2-time-scale r-RESPA integration scheme[44] was used to solve the equations of motion with 2.0 fs for the large time step and 0.4 fs for the intramolecular motions. The Nosé−Hoover thermostat was used to maintain a constant temperature of 300 K.[45,46]

We note that these simulations do not contain a structural diffusion mechanism. However, from the analysis of the hydration structure of the hydronium ions obtained from these simulations we can study the characteristics of Zundel and Eigen ions, which are necessary for structural diffusion.[47,48]

IV. Results and Discussion

In this work, we have divided the simulation box into four regions, as shown in Figure 4. Because the system is periodic in all dimensions (with a period of nominally 12 nm), we have two interfaces in the system. As noted above, the specification of the width of each of these faces, L_z^J, is arbitrary. We have chosen to make the widths of the membrane side of the interface (MI) and vapor side of the interface (VI) 10 Å. This makes the width of the bulk membrane (BM) and bulk vapor (BV) nominally 40 Å. The interfacial width is intentionally an overestimate and is chosen to make sure that all of the interfacial behavior is captured in the interfacial regions. Admittedly, some bulk behavior will also be included in the interfacial region. A quantitative interfacial width is calculated by fitting hyperbolic tangents in the density profiles, as will be discussed later.

We begin the discussion by studying the snapshots of the interfacial region and analyzing the orientation of the hydronium ions at the interface. The various structural measurements, including pair correlation functions, hydronium ion hydration histograms, and density distributions, are studied in the above-mentioned four regions. Then the diffusivities of the water molecules and hydronium ions at the interface are reported.

IV.A. Pair Correlation Functions. As in the previous work,[14] the pair correlation functions (PCFs) were generated for virtually every combination of pairs of atoms in the simulation. In this work, we limit ourselves to reporting the PCF between the O of H_3O^+ and the O of H_2O. What is new in this work is that we report separate PCFs for the four regions of the simulation cell, BM, MI, VI, and BV. The PCF is an

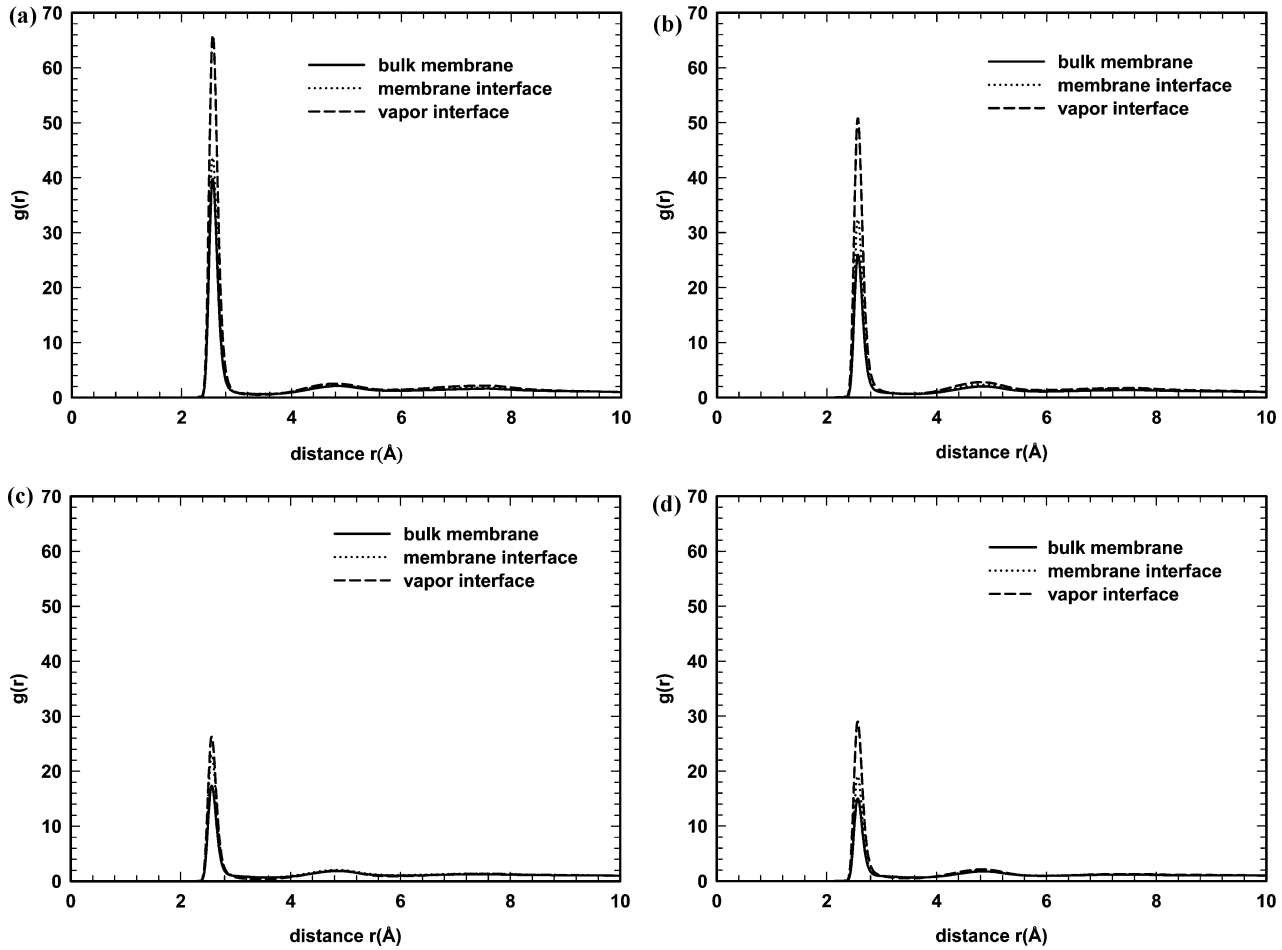

Figure 5. Pair correlation function between the oxygen of the hydronium ion and the oxygen of water molecules at water contents of (a) 5 wt %, (b) 10 wt %, (c) 15 wt %, and (d) 20 wt %. Solid line, bulk membrane; dotted line, membrane interface; and dashed line, vapor interface.

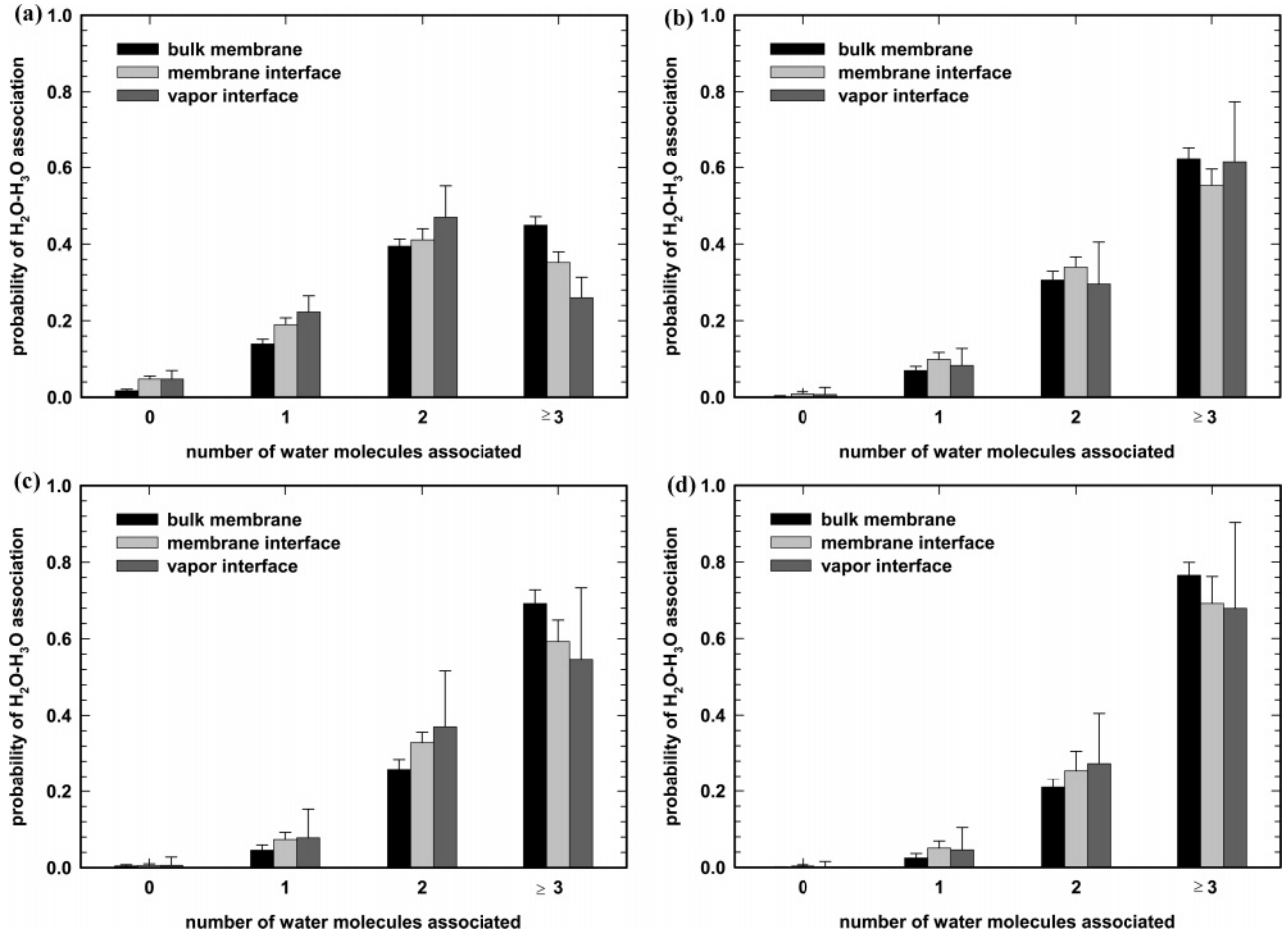

Figure 6. Distribution of hydrated hydronium complexes as a function of hydration number for water contents of (a) 5 wt %, (b) 10 wt %, (c) 15 wt %, and (d) 20 wt %.

unnormalized conditional probability distribution. In homogeneous systems, it is scaled by the bulk density so that the PCF is unity at infinite separation.

In this work, we have an inhomogeneous system with four regions and we report PCFs for each region. In inhomogeneous systems, the bulk density now is a weighted average of the individual phase densities and if used as a scaling factor will not generate PCFs from the different phases that are unity at infinite separation. Therefore, we have scaled each PCF independently so that they individually approach unity at our maximum distance of 10 Å.

In Figure 5a−d, we show the $O_{H_3O^+} - O_{H_2O}$ PCF as a function of the region in the simulation cell and degree of humidity. From these figures, we observe that the first peaks are the same at 2.55 Å in the three regions where hydronium ions are present at 5, 10, 15, and 20 wt % water. The fourth region, the bulk vapor, does not contain any hydronium ions and hence is not shown in the plot. Practically, the third region, which is the vapor side interface, should also not contain any hydronium ions; but because of the roughness of the interface, there is some distribution of molecules around a geometric center of the interface that separates the MI and VI regions. At all water contents, we observe the sharpest first peak in the VI, a first peak of intermediate sharpness in the MI, and the least sharp first peak in the BM region. The second peak is also more pronounced for the interfacial phases. This trend can be tied to the water density, which is decreasing as one moves away from the bulk membrane, as will be discussed shortly. The preferential distribution of water molecules near the hydronium ion is accentuated by lowering the average water density. From an energetic point of view, the relative energetic advantage of being at a nearest-neighbor position is greater as the bulk density decreases. We see a similar effect in the fact that the height of the first peak decreases as the water content is increased.

IV.B. Hydronium Hydration Histograms. The PCFs shown in Figure 5 can be integrated to give the number of water molecules within a specific radial distance. We have chosen to examine the degree of hydration of hydronium ions based on the number of water molecules in which the O of H_2O lies within 3.2 Å of the O of H_3O^+. This distance was chosen as a nominal value of the minimum between the first and second peak of the PCFs in Figure 5. Integrating the same PCF from quantum mechanical simulations of bulk water,[48] we find that the average number of water molecules within 3.2 Å of an H_3O^+ is 3.78.[49] This corresponds generally to an O of H_2O hydrogen-bonding with each of the three H atoms of the H_3O^+, and the O of the H_3O^+ hydrogen-bonding to an H atom of a fourth H_2O.

The probability of finding a fixed number of water molecules around a hydronium ion with a radial distance less than 3.2 Å is shown in Figure 6 as a function of the region within the simulation cell and degree of humidity. From a comparison of Figure 6a−d, we can clearly see that as the water content is increased the hydration distribution is also shifted to higher values in all regions. The probability of finding a hydronium ion with three or more water molecules within 3.2 Å increases with increasing water content. This histogram has relevance to structural diffusion, which requires the existence of Eigen ions, involving the presence of at least three water molecules within 3.2 Å. From the figures, we see that there is a slight decrease in the probability of finding a fully hydrated hydronium ion as

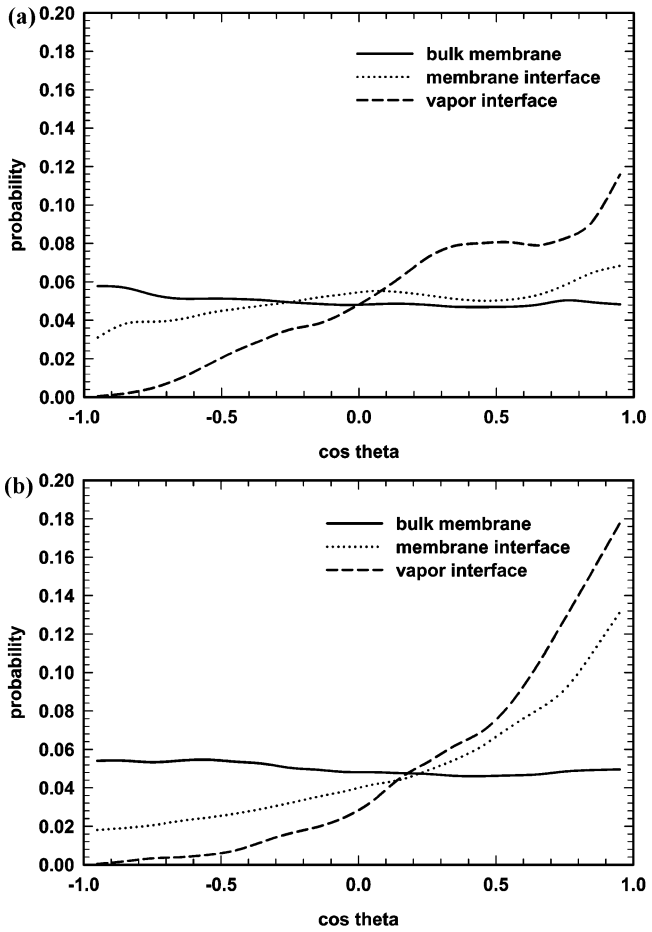

Figure 7. Probability distribution of the orientation of the hydronium ion with respect to the *z* axis (perpendicular to interface) at water contents of (a) 5 wt % and (b) 20 wt %. Solid line, bulk membrane; dotted line, membrane interface; and dashed line, vapor interface.

one approaches the interface, which is present at all levels of humidity. This decrease in probability would correspond to a lower value of the structural diffusivity near the interface.

IV.C. Hydronium Orientation at the Interface. In Figure 7, we present the probability distribution of the orientation of the hydronium ions with respect to the *z* axis (perpendicular to the interface surface). The hydronium axis is defined to originate at the midpoint of the three hydrogen atoms and terminate at the oxygen position. An angle of 0° corresponds to the oxygen atom protruding into the vapor phase. An angle of 180° corresponds to the oxygen atoms buried in the membrane. From the distributions shown in Figure 7, it is clear that the distribution is isotropic in the bulk membrane. However, at the interface, there is a strong preference for the hydronium to be oriented with the oxygen atom protruding into the vapor phase. A snapshot taken normal to the interfacial surface, depicting this configuration, is shown in Figure 8. In this figure, the green spheres represent the oxygen of hydronium. Where one can see green spheres unobscured by the white hydrogen attached to them, those oxygens are sticking out into the vapor phase. There is previous experimental[50,51] and simulation data[52] showing this preferential orientation. The reason for its existence lies in the fact that it is energetically favorable for the hydronium ion to maintain three hydrogen bonds between its hydrogen atoms and the oxygen atom of H_2O in the hydrated membrane.

IV.D. Interfacial Width. In Figure 9, we show the average density profile of water for the four levels of humidity with the zero coordinate on the *x* axis corresponding to the central

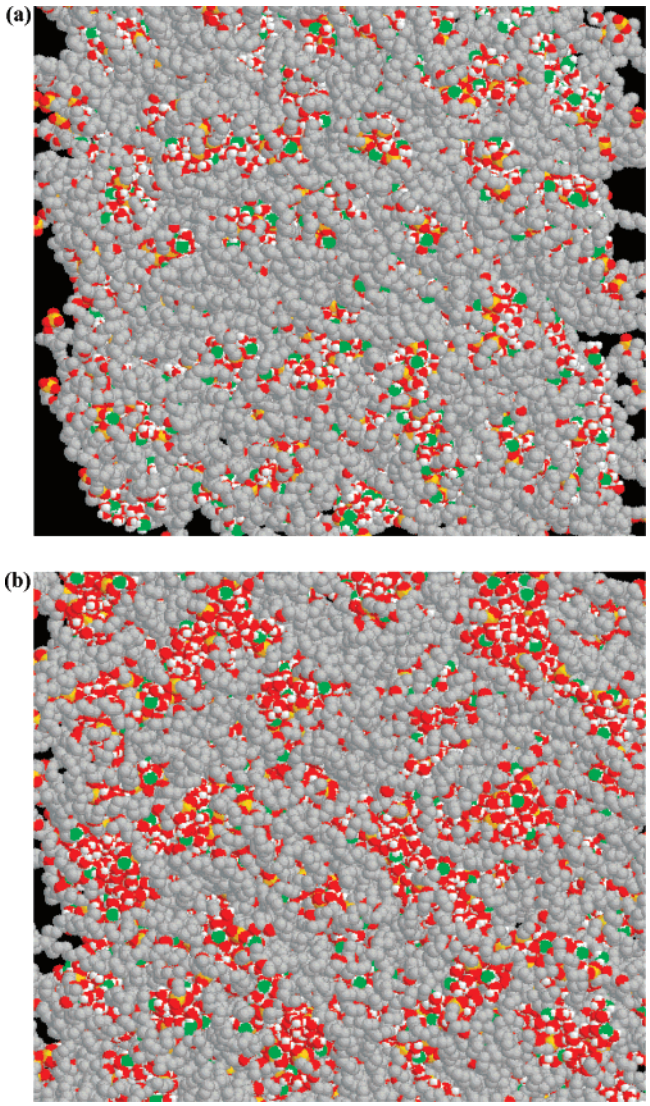

Figure 8. Snapshot taken normal to the interface from a MD simulation of hydrated Nafion at $T = 300$ K and nominal water contents of (a) 5 wt % and (b) 20 wt %. CF_2 and CF_3 pseudo-atoms are gray, H are white, S are orange, and O are red, except the O of H_3O^+, which are green for emphasis.

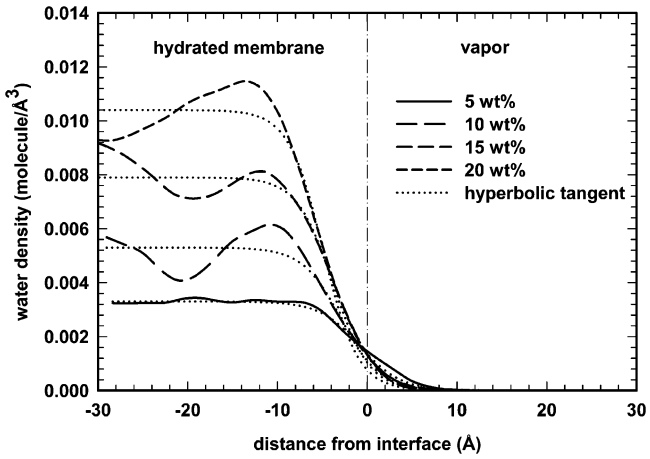

Figure 9. Density profile for water along the *z* direction with the hyperbolic tangent fitted for the water contents of 5 wt %, 10 wt %, 15 wt %, and 20 wt %.

location of the membrane/vapor interface. There is some noise in the water density in the membrane because the system is spatially inhomogeneous on the nanoscale and because simula-

TABLE 2: Interfacial Width at Various Water Contents

water content (wt %)	interfacial width δ (Å)
5	9.0
10	8.6
15	8.0
20	7.7

tions are not long enough to average out this effect completely. It is typical when performing the simulations of two phase systems to fit the density distribution to a hyperbolic tangent, which has four parameters.[53] Three of the parameters, the location of the interface, the BM density, and the BV density, are taken directly from simulation. The fourth parameter, the interfacial width, is fit to the simulation data. The interfacial width calculated is shown in the Table 2. We see that as the humidity increases, the interfacial width decreases. One can understand the decrease in interfacial width with increasing humidity by examining the snapshots of the system taken parallel to the interfacial surface, as shown in Figure 10a at 5 wt % and b at 20 wt %. The surface has a roughness due to the relatively large and inflexible Nafion molecules. This roughness can be smoothed by small water molecules filling in the valleys of the interfacial roughness created by Nafion, resulting in a thinner interface. So the dehydrated region of the membrane near the interface decreases with the increase in water content, leading to a decrease in interfacial width.

IV.E. Interfacial Diffusivities. As derived in Section II, eqs 9−12 provide a means to obtain the parallel and perpendicular components of the self-diffusivity of water and the vehicular portion of the self-diffusivity of the hydronium ion. In Tables 3 and 4, we report the vehicular component of the interfacial diffusivities of the hydronium ion parallel and perpendicular to the surface, respectively. The values of the bulk membrane diffusivities are taken from earlier work.[14] The values of the total two-phase parallel and perpendicular diffusivities were generated in the current work, as were the molecular distributions of molecules among the phases. Equations 11 and 12 were used to generate the interfacial diffusivities. From the tables, we observe that the vehicular component of the hydronium ion parallel to the interface is statistically the same as it is in the bulk membrane.

We do, however, observe that the component perpendicular to the interface is substantially larger than the parallel component. Because the hydronium ions do not enter the vapor phase, there can be no net diffusion of hydronium ions perpendicular to the interface on a macroscopic time scale. The same is not true of the parallel component, in which the membrane is still infinite although periodic. Thus, if we could simulate an infinitely long time, then we would find a zero diffusivity in the perpendicular direction. Here, we are reporting relatively short time diffusivities. (The simulations are nonetheless sufficiently long to establish the linear behavior required in the infinite-time limit of the Einstein relation.) To gauge the length scale associated with this diffusive motion, one can consider that the width of the membrane in these simulations is nominally 60 Å. An estimate of the length scale traveled by hydronium ions on average can be obtained by taking the square root of the final mean square displacements used in the determination of the diffusivity. These final MSDs correspond to a length between 9 and 20 Å. This is thus a measure of dynamics on the nanosecond time scale, as opposed to a macroscopic time scale. On a nanoscopic time scale, we observe enhanced diffusivity perpendicular to the interface. This may be a result of the density gradient that exists in the direction perpendicular

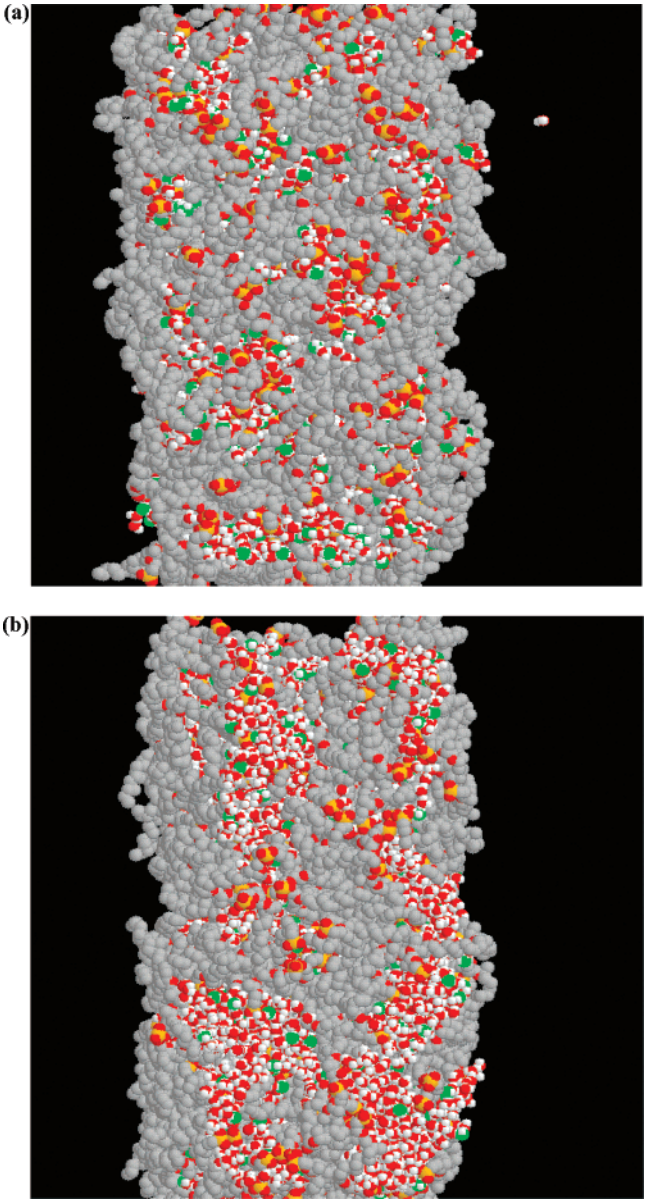

Figure 10. Snapshot taken parallel to the interface from a MD simulation of hydrated Nafion at $T = 300$ K and nominal water contents of (a) 5 wt % and (b) 20 wt %. CF_2 and CF_3 pseudo-atoms are gray, H are white, S are orange, O are red, except the O of H_3O^+, which are green for emphasis.

to the interface, as shown in Figure 9. In short, we see no observable additional resistance to mass transport of the vehicular component of the hydronium ion due to the interface.

We have used eqs 9 and 10 to evaluate the diffusivity of water parallel and perpendicular to the interface. Water differs from the hydronium ion in that it is present in the vapor phase. In this work, the diffusivity of water in the bulk vapor phase, D^{BV}, is assumed to be 0.1 cm^2/s, a reasonable estimate of the diffusivity of a gas at room temperature and pressure.

From Table 5 we can see that perpendicular component of the interfacial diffusivity of the water displays the same behavior as that observed for the hydronium ions, namely, that it increases with humidity and is greater than the diffusivity in the bulk membrane. Thus, we do not see an inherent additional mass transfer resistance to water through the membrane/vapor interface.

The simulations were unable to generate a statistically reliable diffusivity for water parallel to the interface. There are statisti-

TABLE 3: Diffusion Coefficient of Hydronium Ions in the Interfacial Region, Parallel to the Interface[a]

water content (wt %)	$D_{\|\|}^{BM}$ (10^{-11} m^2/s)	$D_{\|\|}^{T}$ (10^{-11} m^2/s)	$\chi_{H_3O^+}^{BM}$ (no units)	$\chi_{H_3O^+}^{I}$ (no units)	$D_{\|\|}^{I}$ (10^{-11} m^2/s)
5	2.97	3.63	0.635	0.365	4.79
10	6.36	6.19	0.683	0.317	6.33
15	14.73	16.04	0.699	0.301	19.07
20	25.23	27.04	0.717	0.282	31.64

[a] $D_{||}^{BM}$, $D_{||}^{T}$, $D_{||}^{I}$: bulk membrane and total and interfacial diffusivity of the hydronium ions parallel to the interface. $\chi_{H_3O^+}^{BM}$, $\chi_{H_3O^+}^{I}$: fraction of hydronium ions in the bulk membrane and interfacial region.

TABLE 4: Diffusion Coefficient of Hydronium Ions in the Interfacial Region, Perpendicular to the Interface[a]

water content (wt %)	$D_{\perp}^{BM}$ (10^{-11} m^2/s)	$D_{\perp}^{T}$ (10^{-11} m^2/s)	$\chi_{H_3O^+}^{BM}$ (no unit)	$\chi_{H_3O^+}^{I}$ (no unit)	ψ_z^{BM} (no unit)	ψ_z^{I} (no unit)	$D_{\perp}^{I}$ (10^{-11} m^2/s)
5	2.97	3.37	0.635	0.365	0.491	0.509	39.17
10	6.36	5.30	0.683	0.317	0.500	0.500	21.45
15	14.73	13.51	0.699	0.301	0.511	0.489	66.58
20	25.23	21.08	0.717	0.282	0.520	0.480	90.81

[a] $D_{\perp}^{BM}$, $D_{\perp}^{T}$, $D_{\perp}^{I}$: bulk membrane and total and interfacial diffusivity of the hydronium ions perpendicular to the interface. $\chi_{H_3O^+}^{BM}$, $\chi_{H_3O^+}^{I}$: fraction of hydronium ions in the bulk membrane and interfacial region. ψ_z^{BM}, ψ_z^{I}: length fraction of the bulk membrane and interfacial region.

TABLE 5: Diffusion Coefficient of Water in the Interfacial Region, Perpendicular to the Interface[a]

water (wt %)	$D_{\perp}^{BM}$ (10^{-10} m^2/s)	$D_{\perp}^{T}$ (10^{-10} m^2/s)	$D_{\perp}^{BV}$ (10^{-5} m^2/s)	$\chi_{H_2O}^{BM}$	$\chi_{H_2O}^{I}$	$\chi_{H_2O}^{BV}$	ψ_z^{BM}	ψ_z^{I}	ψ_z^{BV}	$D_{\perp}^{I}$ (10^{-10} m^2/s)
5	1.39	2.05	1.00	0.666	0.333	0.001	0.329	0.341	0.329	8.43
10	3.75	3.04	1.00	0.714	0.284	0.002	0.334	0.333	0.334	6.49
15	7.37	4.86	1.00	0.764	0.235	0.001	0.338	0.324	0.338	12.26
20	9.40	6.24	1.00	0.792	0.207	0.001	0.342	0.316	0.342	21.01

[a] $D_{\perp}^{BM}$, $D_{\perp}^{T}$, $D_{\perp}^{BV}$, $D_{\perp}^{I}$: bulk membrane, total, bulk vapor, and interfacial diffusivity of the water perpendicular to the interface. $\chi_{H_2O}^{BM}$, $\chi_{H_2O}^{I}$, $\chi_{H_2O}^{BV}$: fraction of water in the bulk membrane, interfacial, and bulk vapor region. ψ_z^{BM}, ψ_z^{I}, ψ_z^{BV}: length fraction of the bulk membrane, interfacial, and bulk vapor region.

cally very few water molecules in the vapor phase. In defining the simulation volume, there are two choices. If there is a large vapor-phase that allows many water molecules in the vapor phase, then we obtain good statistics on the vapor properties (which are not interesting), but this will alter the bulk water content of the hydrated membrane. Alternatively, our choice was to simulate a small vapor phase, while maintaining the same nominal water density in the hydrated membrane. This manifested in an inability to extract a statistically (or physically) meaningful value of the diffusion coefficient of water parallel to the interface. Hence, we do not report values for the diffusion coefficient of water parallel to the interface. However, based on the past relationship between the water and hydronium diffusivities in the bulk membrane region, it is not unreasonable to infer that the parallel component of the diffusivity of water is similar to that in the bulk phase, as was the case with the hydronium ion.

V. Conclusions

We have performed molecular dynamics simulations and examined the structural and transport properties of water and hydronium ions at the interface of a Nafion polymer electrolyte membrane and a vapor phase. We studied systems at 5%, 10%, 15%, and 20% water content by weight at 300 K. The diffusivities of the hydronium ions and water molecules increase with water content. We have reported interfacial water and hydronium ion vehicular diffusion components parallel and perpendicular to the interface. For hydronium ions, the perpendicular components are much higher than the parallel component. The parallel component is almost equal to that of the bulk hydrated membrane. At the nanosecond scale, the perpendicular component of the vehicular diffusivity is large, likely due to the density gradient at the interface. At the macro time scale, the absence of hydronium ions in the vapor phase implies that there is no net diffusion of the ions perpendicular to the interface. For water, we found qualitatively similar diffusive behavior except that water can certainly exist in the vapor phase. From these diffusivities, we can conclude that there is no inherent resistance to the vehicular diffusion of the hydronium ions and water due to the interface. However, we found that there was a decrease in the fraction of fully hydrated hydronium ions at the interface. This translates into a lower probability of forming Eigen ions, which are necessary for structural diffusion. This finding is consistent with a water depletion region at the membrane/vapor interface that is less than a nanometer wide. The structural measurements such as the pair correlation function showed that the association of water molecules with the hydronium ion increases as the average water density decreases. This can be observed by the monotonic decrease in the peak height as the water content increases and also as one moves from the vapor interfacial region to the bulk membrane. From the average density profile of water, we concluded that the thickness of the interface decreases with increasing humidity. Finally, we observed that the hydronium ions displayed a preferential orientation at the interface, with their oxygen atoms exposed to the vapor phase.

Acknowledgment. The work is supported by a grant from the U.S. Department of Energy BES under the contract number DE-FG02-05ER15723. This research used resources of the Center for Computational Sciences at Oak Ridge National Laboratory, which is supported by the Office of Science of the DOE under Contract DE-AC05-00OR22725.

References and Notes

(1) Kreuer, K.-D.; Paddison, S. J.; Spohr, E.; Schuster, M. *Chem. Rev.* **2004**, *104*, 4637.
(2) O'Hayre, R.; Prinz, F. B. *J. Electrochem. Soc.* **2004**, *151*, A756.
(3) Xie, J.; More, K. L.; Zawodzinski, T. A.; Smith, W. H. *J. Electrochem. Soc.* **2004**, *151*, A1841.
(4) Hsu, W. Y.; Gierke, T. D. *J. Membr. Sci.* **1983**, *13*, 307.
(5) Verbrugge, M. W.; Hill, R. F. *J. Electrochem. Soc.* **1990**, *137*, 886.
(6) Falk, M. *Can. J. Chem.* **1980**, *58*, 1495.
(7) Vishnyakov, A.; Neimark, A. V. *J. Phys. Chem. B* **2001**, *105*, 9586.
(8) Rivin, D.; Meermeier, G.; Schneider, N. S.; Vishnyakov, A.; Neimark, A. V. *J. Phys. Chem. B* **2004**, 8900.
(9) Petersen, M. K.; Wang, F.; Blake, N. P.; Metiu, H.; Voth, G. A. *J. Phys. Chem. B* **2005**, *109*, 3727.
(10) Petersen, M. K.; Voth, G. A. *J. Phys. Chem. B* **2006**, *110*, 18594.
(11) Spohr, E.; Commer, P.; Kornyshev, A. A. *J. Phys. Chem. B* **2002**, *106*, 10560.
(12) Commer, P.; Cherstvy, A. G.; Spohr, E.; Kornyshev, A. A. *Fuel Cells* **2002**, *2*, 127.
(13) Jang, S. S.; Molinero, V.; Cagin, T.; Goddard, W. A. *J. Phys. Chem. B* **2004**, *108*, 3149.
(14) Cui, S. T.; Liu, J. W.; Selvan, M. E.; Keffer, D. J.; Edwards, B. J.; Steele, W. V. *J. Phys. Chem. B* **2007**, *111*, 2208.
(15) Paddison, S. J.; Zawodzinski, T. A. *Solid State Ionics* **1998**, *113*−115, 333.
(16) Paddison, S. J.; Pratt, L. R.; Zawodzinski, T. A. *J. New Mater. Electrochem. Sys.* **1999**, *2*, 183.
(17) Paddison, S. J.; Paul, R.; Zawodzinski, T. A. *J. Electrochem. Soc.* **2000**, *147*, 617.
(18) Paddison, S. J.; Paul, R.; Zawodzinski, T. A. *J. Chem. Phys.* **2001**, *115*, 7753.
(19) Paul, R.; Paddison, S. J. *J. Chem. Phys.* **2001**, *115*, 7762.
(20) Eikerling, M.; Paddison, S. J.; Zawodzinski, T. A. J. *J. New Mater. Electrochem. Sys.* **2002**, *5*, 15.
(21) Paddison, S. J.; Paul, R.; Kreuer, K.-D. *Phys. Chem. Chem. Phys.* **2002**, *4*, 1151.
(22) Paddison, S. J.; Paul, R. *Phys. Chem. Chem. Phys.* **2002**, *4*, 1158.
(23) Paddison, S. J. *Annu. Rev. Mater. Res.* **2003**, *33*, 289.
(24) Paddison, S. J.; Elliott, J. A. *J. Phys. Chem. A* **2005**, *109*, 7583.
(25) Paul, R.; Paddison, S. J. *J. Chem. Phys.* **2005**, *123*, 224704.
(26) Paddison, S. J.; Elliott, J. A. *Phys. Chem. Chem. Phys.* **2006**, *8*, 2193.
(27) Urata, S.; Irisawa, J.; Takada, A.; Shinoda, W.; Tsuzuki, S.; Mikami, M. *J. Phys. Chem. B* **2005**, *109*, 4269.
(28) Venkatnathan, A.; Devanathan, R.; Dupuis, M. *J. Phys. Chem. B* **2007**, *111*, 7234.
(29) Choi, P.; Jalani, N. H.; Datta, R. *J. Electrochem. Soc.* **2005**, *152*, A1548.
(30) Janssen, G. J. M. *J. Electrochem. Soc.* **2001**, *148*, A1313.
(31) Zawodzinski, T. A.; Derouin, C.; Radzinski, S.; Sherman, R. J.; Smith, V. T.; Springer, T. E.; Gottesfeld, S. *J. Electrochem. Soc.* **1993**, *140*, 1041.
(32) Hirunsit, P.; Balbuena, P. B. *J. Phys. Chem. C* **2007**, *111*, 1709.
(33) Yan, W. M.; Chu, H. S.; Chen, J. Y.; Soong, C. Y.; Chen, F. L. *J. Power Sources* **2006**, *162*, 1147.
(34) Bernardi, D. M.; Verbrugge, M. W. *AIChE J.* **1991**, *37*, 1151.
(35) Liu, J. W.; Selvan, M. E.; Cui, S. T.; Edwards, B. J.; Keffer, D. J.; Steele, W. V. *J. Phys. Chem. C*, submitted for publication, 2007.
(36) Allen, M. P.; Tildesley, D. J. *Computer Simulation of Liquids*; Oxford Science Publications: Oxford, 1987.
(37) Haile, J. M. *Molecular Dynamics Simulation*; John Wiley & Sons, Inc.: New York, 1992.
(38) Gubbins, K. E. Thermal Transport Coefficients for Dense Fluids. In *A Specialist Periodical Report. Statistical Mechanics*; Singer, K., Ed.; Burlington House: London, 1973; Vol. 1, p 194.
(39) Steele, W. A. Time Correlation Functions. In *Transport Phenomena in Fluids*; Hanley, H. J. M., Ed.; Dekker: New York, 1969; p 209.
(40) Keffer, D.; Adhangale, P. *Chem. Eng. J.* **2004**, *100*, 51.
(41) Darken, L. S. *Trans. Am. Inst. Min. Metall. Eng.* **1948**, *175*, 184.
(42) Keffer, D.; Adhangale, P.; Edwards, B. J. *J. Non-Newtonian Fluid Mech.* **2004**, *120*, 41.
(43) Keffer, D. J.; Gao, C. Y.; Edwards, B. J. *J. Phys. Chem. B* **2005**, *109*, 5279.
(44) Tuckerman, M.; Berne, B. J.; Martyna, G. J. *J. Chem. Phys.* **1992**, *97*, 1990.
(45) Nosé, S. *Mol. Phys.* **1984**, *52*, 255.
(46) Hoover, W. G. *Phys. Rev. A* **1985**, *31*, 1695.
(47) Agmon, N. *Chem. Phys. Lett.* **1995**, *244*, 456.
(48) Tuckerman, M.; Laasonen, K.; Sprik, M.; Parrinello, M. *J. Chem. Phys.* **1995**, *103*, 150.
(49) Brancato, G.; Tuckerman, M. E. *J. Chem. Phys.* **2005**, *122*.
(50) Miranda, P. B.; Shen, Y. R. *J. Phys. Chem. B* **1999**, *103*, 3292.
(51) Raduge, C.; Pflumio, V.; Shen, Y. R. *Chem. Phys. Lett.* **1997**, *274*, 140.
(52) Petersen, M. K.; Iyengar, S. S.; Day, T. J. F.; Voth, G. A. *J. Phys. Chem. B* **2004**, *108*, 14804.
(53) Chen, Y.; Aranovich, G. L.; Donohue, M. D. *J. Colloid Interface Sci.* **2007**, *307*, 34.